Organic & Biomolecular Chemistry

ROYAL SOCIETY OF CHEMISTRY

PAPER

View Article Online
View Journal | View Issue

Cite this: *Org. Biomol. Chem.*, 2021, **19**, 6546

Photosensitizer–peptoid conjugates for photoinactivation of Gram-negative bacteria: structure–activity relationship and mechanistic studies†

Woojin Yang,‡[a] Younggun Yoon,‡[b] Yunjee Lee,‡[a] Hyeongyeol Oh,‡[a] Jieun Choi,[a] Sujin Shin,[b] Seongsoo Lee,[c] Hohjai Lee,[a] Yunho Lee *[b] and Jiwon Seo *[a]

Received 11th May 2021,
Accepted 9th July 2021

DOI: 10.1039/d1ob00926e

rsc.li/obc

Multitarget engagement is considered an effective strategy to overcome the threat of bacterial infection, and antimicrobials with multiple mechanisms of action have been successful as natural chemical weaponry. Here, we synthesized a library of photosensitizer-peptoid conjugates (PsPCs) as novel antimicrobial photodynamic therapy (aPDT) agents. The peptoids, linkers, and photosensitizers were varied, and their structure-antimicrobial activity relationships against *Escherichia coli* were evaluated; PsPC **9** was indicated to be the most promising photoresponsive antimicrobial agent among the synthesized PsPCs. Spectroscopic analyses indicated that **9** generated singlet oxygen upon absorption of visible light (420 nm) while maintaining the weakly helical conformation of the peptoid. Mechanistic studies suggested that damage to the bacterial membrane and cleavage of DNA upon light irradiation were the main causes of bactericidal activity, which was supported by flow cytometry and DNA gel electrophoresis experiments. We demonstrated that the optimal combination of membrane-active peptoids and photosensitizers can generate an efficient aPDT agent that targets multiple sites of bacterial components and kills bacteria by membrane disruption and reactive oxygen species generation.

Introduction

Multitarget antimicrobials have been preferentially used in nature as host-defense weaponry.[1] This multitarget strategy has been used to minimize resistance development and has proven to be effective in the clinic, as exemplified by long-established antibiotics such as penicillins[2] and polymyxin B.[3] More recently, a multitarget strategy has been adopted with various investigational antibiotic drugs by conjugating two known antibiotics with different mechanisms of action. Stable hybrids of vancomycin–cephalosporin (cefilavancin[4] and TD-1607[5]), quinolone–oxazolidinone (cadazolid[6] and MCB3681[7]), and rifamycin–quinolone (TNP-2092[8]) are in clinical trials against antibiotic-resistant strains.

Antimicrobial peptides (AMPs) often take advantage of this multitarget approach. As a molecule produced by the innate immune system, nature has utilized AMPs as a first-line defense against invading pathogens. More than 5000 AMPs have been discovered to date, including peptides used in their natural form and rationally designed artificial peptides.[9] The activity of AMPs originates from their structural characteristics that can damage multiple components of a bacterial cell. For example, cationic AMPs such as cathelicidin (LL-37),[10] magainin-2,[11] and lactoferrin[12] have both cationic and hydrophobic residues, forming an amphipathic α-helical conformation. This structural feature allows electrostatic interactions with the negatively charged bacterial membrane components, including teichoic acid (cell wall, Gram-positive bacteria) or the phospholipid head groups of the bacterial membrane, leading to the subsequent destruction of bacterial barriers.[13] Recent studies have also reported cationic AMPs that target intracellular nucleic acids and proteins, demonstrating nature's preference for a multi-effective mechanism.[14] However, despite their potential, only seven AMPs have been approved by the FDA thus far, with four of them being vancomycin or its derivatives

[a]*Department of Chemistry, Gwangju Institute of Science and Technology, 123 Cheomdan-gwagiro, Buk-gu, Gwangju 61005, South Korea. E-mail: jseo@gist.ac.kr*
[b]*School of Earth Sciences and Environmental Engineering, Gwangju Institute of Science and Technology, 123 Cheomdan-gwagiro, Buk-gu, Gwangju 61005, South Korea. E-mail: yhlee42@gist.ac.kr*
[c]*Gwangju Center, Korea Basic Science Institute (KBSI), 49 Dosicheomdansaneopro, Nam-gu, Gwangju 61751, South Korea*

†Electronic supplementary information (ESI) available: Synthetic procedure for photosensitizers, peptoids, and PsPCs; HPLC data and ESI-MS data for **1–16**; the results of additional photoinactivation studies, circular dichroism spectra, and flow cytometry experiments; and cytotoxicity of **9**, **14**, and **16**. See DOI: 10.1039/d1ob00926e

‡These authors contributed equally to this work.

and the other three being gramicidin, daptomycin, and colistin.[15] Therefore, researchers have focused on various strategies to overcome the limitations of AMPs (*e.g.*, a short plasma half-life)[15] by incorporating unnatural amino acids,[16] modulating the length of the AMP,[17] or cyclizing the sequence.[18]

Antimicrobial photodynamic therapy (aPDT) was introduced in the early 20th century[19] and has been rediscovered as a promising multitarget strategy to fight against recent widespread multidrug resistant pathogens.[20] aPDT utilizes reactive oxygen species (ROS) generated by a photosensitizer during light irradiation. Different types of radical species (*i.e.*, $^{\bullet}OH$, $O_2^{\bullet-}$) or singlet oxygen ($^1O_2$) are produced during this process through the type I and type II pathways, respectively.[21] The generated ROS can cause fatal damage to multiple sites in bacteria, including membrane components[22] and intracellular biomass (*e.g.*, nucleic acids and proteins).[23,24] Therefore, various types of photosensitizers have been developed, including phenothiazinium,[25] tetrapyrroles (*i.e.*, porphyrin,[26] chlorin,[27] and phthalocyanine[28]), and riboflavin.[29] Researchers have focused on increasing the efficiency of aPDT by introducing photosensitizers into biomaterials, such as celluloses,[30] cyclodextrins,[31] and aptamers.[32]

The combination of an AMP and a photosensitizer has demonstrated strong synergistic effects caused by targeting the bacterial membrane while simultaneously generating toxic ROS. The potential of this approach was actively demonstrated by Gobbo and coworkers with their porphyrin–AMP conjugates.[33,34] AMPs such as apidaecin 1b, magainin, and buforin were linked to porphyrinoids, and these photosensitizer–peptide conjugates induced the death of bacterial cells upon light irradiation. Sol and coworkers expanded the applications of porphyrin–peptide conjugates using cationic porphyrin and the macrocyclic antibiotic polymyxin B, which is active against only Gram-negative bacteria.[35,36] The conjugate cationic porphyrin–polymyxin B exhibited antimicrobial activity against both Gram-positive and Gram-negative strains, overcoming the limitations of the peptide acting alone. Photosensitizers conjugated with other peptides, such as lipopolysaccharide-binding peptide,[37] oligoarginine,[38] and tat peptide,[39] have also demonstrated the effectiveness of this approach. Nevertheless, this strategy needs to be further explored by employing various types of membrane-active peptides and peptidomimetics to take full advantage of this strategy.

Among peptidomimetics, peptoids or *N*-substituted glycine oligomers have attracted attention as promising antimicrobial agents. Antimicrobial peptoids have several advantages that originate from their structural features and synthetic processes. Peptoid structures are composed of a repeating tertiary amide backbone that provides increased stability towards proteolytic degradation.[40] The peptoid sequence can be elongated *via* a submonomer method, which enables various side chain incorporations in a sequence-specific manner.[41,42] Cationic and hydrophobic residues can be precisely located at specific positions covering a wide spectrum of physicochemical and conformational properties. Representative examples are the cationic amphipathic peptoids that mimic the structural features of the natural AMP magainin-2, invented by Barron and coworkers.[43] These α-helical peptoids showed broad-spectrum antimicrobial activity against both Gram-positive and Gram-negative bacteria in the low micromolar range.[44,45] Follow-up studies have reported the preparation of various antimicrobial peptoids through tuning the cationic charge and hydrophobicity,[46,47] introducing heterocyclic rings,[48,49] as well as adopting different scaffolds such as peptide–peptoid hybrids[50] and cyclic peptoids.[51] The effects of the conformational flexibility of peptoids on their antimicrobial activity were investigated by a method called helicity modulation.[52] Therein, a peptoid with moderate helicity showed the most dramatic increase in selectivity, maintaining its antimicrobial activity. Unlike peptides, peptoid scaffolds offer a unique advantage of evaluating the structure–activity relationship by modulating their secondary structure while maintaining the physicochemical properties (*e.g.*, cationic charge and hydrophobicity). Thus, introduction of peptoids with varying degree of helicity (*e.g.*, fully helical, non-helical, and moderately helical) into the aPDT system would facilitate the discovery of optimal conformation that has strong interaction with bacterial membrane and has a synergistic antimicrobial activity upon conjugation with a photosensitizer.

In the present study, we introduce a new type of peptoid-based aPDT agent: a photosensitizer–peptoid conjugate (PsPC). Several types of porphyrins, chlorins, and helicity-modulated peptoids were adopted for the design of our PsPC library. The PsPCs were expected to localize on the bacterial membrane or penetrate the membrane, followed by the generation of singlet oxygen during visible light irradiation, which consequently leads to the death of the target bacteria. Photosensitizers with either carboxylic acid or primary amine functional groups have been successfully conjugated to antimicrobial peptoids, whose helical integrity is controlled by the helix-inducing peptoid monomers. The antimicrobial activities of the prepared set of PsPCs were screened by counting the colony-forming units (CFUs) and determining the minimum inhibitory concentration (MIC) of each PsPC. Further investigation was conducted by spectroscopic and bioanalytical methods, including UV-vis, fluorescence, phosphorescence, circular dichroism (CD), flow cytometry, and gel electrophoresis, to determine the origin of the photoresponsive activity of selected PsPCs. PsPCs with unique photophysical and conformational characteristics could provide insight for ongoing research on antimicrobial peptoid development and aPDT agent design.

Results and discussion

Synthesis of PsPCs

PsPCs were designed to have each of the components, namely photosensitizer and peptoid, connected by a linker (Fig. 1 and Scheme S1†). Two porphyrins (*meso*-tetra(4-*N*-methylpyridyl) porphine (TMPyP), tetraphenylporphyrin (TPP)) and three

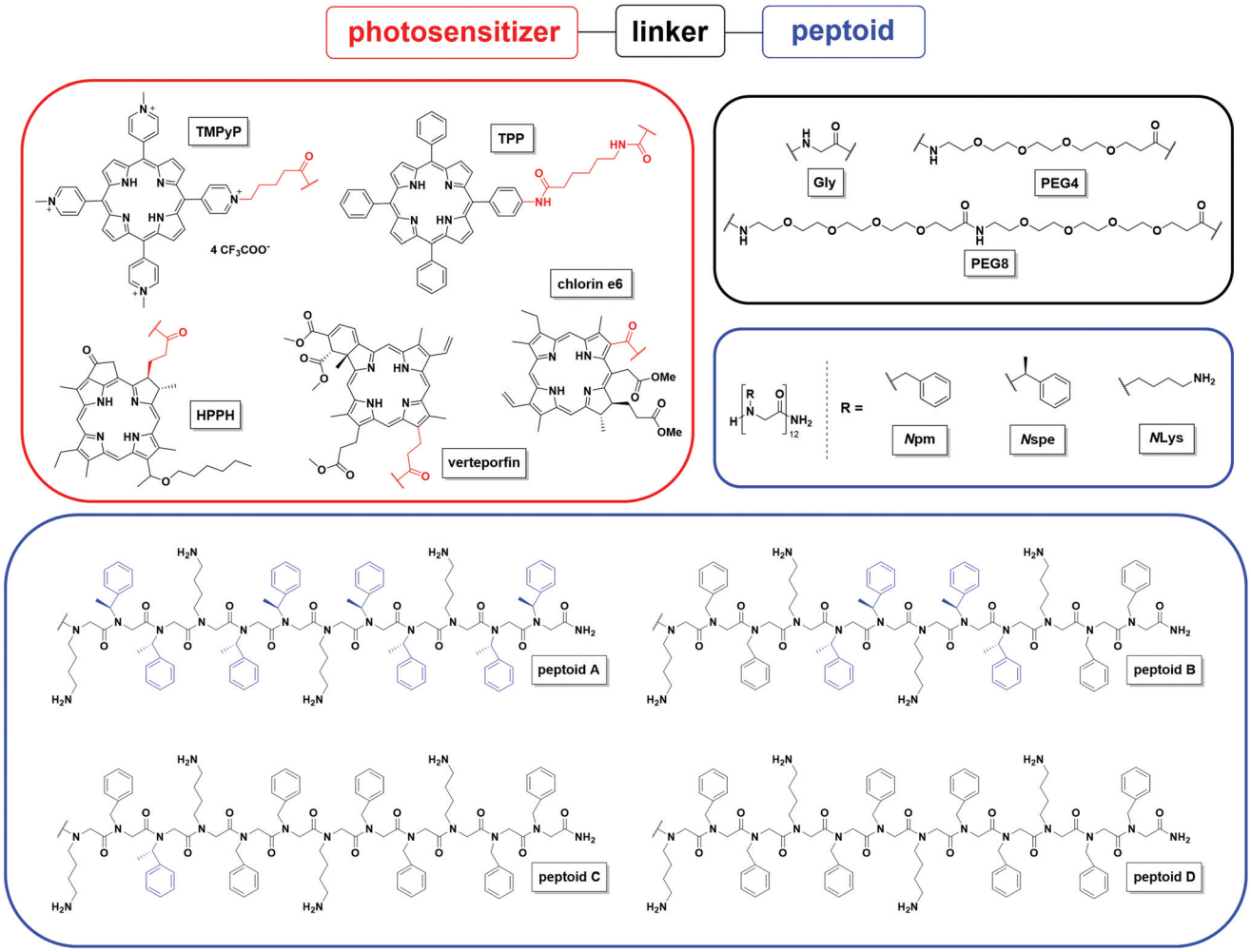

Fig. 1 Structures of photosensitizers, linkers, and peptoids.

chlorins (2-[1-hexyloxyethyl]-2-devinyl pyropheophorbide-a (HPPH), verteporfin, chlorin e6) were selected as photosensitizers, each of which is known to generate singlet oxygen upon visible light irradiation (Fig. 1, red box).[53] Cationic TMPyP and hydrophobic TPP are *meso*-substituted porphyrins that are functionalized with a carboxylic acid or a primary amine, respectively, for peptoid conjugation. The other three compounds, the chlorins, have been investigated in the clinic for anticancer photodynamic therapy. HPPH has been evaluated for multiple tumor types, including esophageal cancers.[54] Verteporfin has been used for the treatment of age-related macular degeneration.[54] Chlorin e6 was formulated with polyvinylpyrrolidone (PVP), and chlorin e6-PVP induces apoptosis of malignant tumors after localization in the mitochondria and lysozymes.[55] HPPH, verteporfin, and chlorin e6 were prepared as NHS esters to facilitate peptoid conjugation.

Peptoids A–D were used as membrane-active antimicrobial agents (Fig. 1, blue box).[41,43] Previous studies have revealed that the unique conformational feature, a polyproline type I (PPI)-like helix with three residues per turn, is a result of the incorporation of chiral aromatic side chains (*i.e.*, (*S*)-(−)-1-phenylethylamine, *N*spe).[56,57] The degree of helicity can be modulated by the substitution of chiral *N*spe monomers with achiral monomers (*i.e.*, benzylamine, *N*pm).[52,58] Depending on the degree of unfolding, moderately helical peptoids could better distinguish between bacterial and eukaryotic membranes, leading to more selective antimicrobial peptoids.[52] All four peptoids A–D have a fixed number of cationic residues (*i.e.*, 1,4-diaminobutane, *N*Lys), but the position-specific incorporation of helix-inducing *N*spe monomers resulted in different degrees of helicity. Peptoids A and D have fully α-helical and nonhelical conformations, respectively.[43] The degree of folding of peptoids B and C are between the fully helical and nonhelical, with peptoid B showing moderate helicity and peptoid C being weakly helical.[52]

The photosensitizers and peptoids were conjugated using different linkers, glycine (Gly) and polyethylene glycol (PEG4 and PEG8) (Fig. 1, black box). The linkers were attached to the *N*-terminus of each resin-bound peptoid and conjugated with the photosensitizer through an amide bond (Scheme S1†). Diglycine (Gly–Gly) and 6-aminohexyl linkers were also tested; however, these linkers were not optimal, and poor anti-

Table 1 Antimicrobial activity of **1–16** against *S. aureus* (ATCC 25923) and *E. coli* (ATCC 25922)

				S. aureus			*E. coli*		
				MIC[b] (μM)		MBC[b] (μM)	MIC[b] (μM)		MBC[b] (μM)
Compd	PS[a]	Linker	Peptoid	Dark	Light[c]	Light[c]	Dark	Light[c]	Light[c]
1	TMPyP	Gly	A	6.3	6.3	6.3	12.5	12.5	12.5
2	TPP	Gly	A	>25	>25	>25	>25	>25	>25
3	HPPH	Gly	A	>25	>25	>25	>25	>25	>25
4	Verteporfin	Gly	A	>25	>25	>25	>25	>25	>25
5	Chlorin e6	Gly	A	>25	>25	>25	>25	>25	>25
6	TMPyP	PEG4	A	3.1	6.3	6.3	6.3	6.3	6.3
7	TMPyP	PEG8	A	6.3	6.3	12.5	12.5	12.5	12.5
8	TMPyP	Gly	B	6.3	6.3	12.5	6.3	6.3	6.3
9	TMPyP	Gly	C	6.3	6.3	6.3	6.3	1.6	1.6
10	TMPyP	Gly	D	12.5	6.3	25	6.3	3.1	3.1
11	TMPyP	PEG4	C	nd[d]	nd[d]	nd[d]	3.1	3.1	3.1
12	—	—	A	1.6	1.6	3.1	3.1	3.1	3.1
13	—	—	B	3.1	3.1	12.5	6.3	6.3	6.3
14	—	—	C	6.3	6.3	12.5	12.5	12.5	6.3
15	—	—	D	6.3	6.3	25	12.5	12.5	12.5
16	TMPyP	—	—	>25	>25	>25	>25	>25	>25

[a] Photosensitizer. [b] The minimum inhibitory concentration (MIC) and minimum bactericidal concentration (MBC) data represent the mean values of three independent experiments. [c] The samples were irradiated under blue light for 15 min (390–460 nm, 420 nm max, 15.1 J cm^{-2}). [d] Not determined.

microbial activity was observed (data not shown). In peptoids A–D, three linkers and five photosensitizers were combined to find the PsPC with optimal biological activity (**1–11** in Table 1). Peptoids A–D, without photosensitizer conjugation (**12–15** in Table 1), were prepared for comparison. Each compound was purified by preparative HPLC (>97%) and characterized using ESI-MS (Fig. S1, S2 and Table S1†).

Antimicrobial activity of PsPCs

The photoresponsive antimicrobial activity of PsPCs was evaluated by measuring the minimum inhibitory concentration (MIC) and minimum bactericidal concentration (MBC). Blue light irradiation was applied for 15 min with a homemade LED array (390–460 nm, 420 nm max, 16.8 mW cm^{-2}). It was confirmed that the growth of bacterial cells in the absence of PsPCs was not affected under these conditions (Fig. S3†). Several PsPCs (*e.g.*, **6**, **8–11**) exhibited potent antimicrobial activity against *S. aureus* and *E. coli* (Table 1). Notably, PsPC **9** and **10** showed more potent antimicrobial activity against Gram-negative *E. coli* than Gram-positive *S. aureus*. For Gram-positive bacteria, none of PsPCs (**1–10**) showed better antimicrobial activity than peptoid alone (**12**), and no benefit of photosensitizer conjugation was found. Thus, further analysis and discussion were focused on using PsPC as an aPDT agent against *E. coli*.

The antimicrobial activities of PsPCs based on peptoid A (**1–7**) were lower than those of peptoid alone (**12**) under both dark and light conditions (Table 1). Among the five photosensitizers, only cationic TMPyP appeared to be effective when conjugated with a peptoid. The MICs and MBCs of **2–5** were larger than 25 μM, while those of **1** were both 12.5 μM. The decreased antimicrobial activity in compounds **2–5** can be accounted for by the presence of a neutral photosensitizer. Considering that the N- or *C*-terminus of the peptoid helix is inserted into the phospholipid membrane,[43] the interaction between the peptoid and bacterial membrane, with a net negative surface charge, was hampered by the presence of a bulky neutral photosensitizer. However, TMPyP with four permanent cationic charges appears to have a better interaction with the bacterial membrane, leading to increased antimicrobial activity. Thus, TMPyP was selected among the five photosensitizers, and the effect of changing the linker and peptoid was subsequently investigated. A PEG linker (or spacer) was introduced to increase the distance between the bulky photosensitizer and the antimicrobial peptoid. The MICs and MBCs of **6** and **7** were not dramatically different from those of **1** (*i.e.*, 12.5 μM), indicating that the linker may not play a key role in the optimal PsPC.

Variation in the peptoids resulted in a more significant enhancement in antimicrobial activity. The MICs and MBCs of conjugates **8–10** were 6.3 μM or lower, whereas those of the corresponding peptoids themselves (**13–15**) were 6.3 μM or higher. Interestingly, PsPC **9** and **10** showed further enhancement in antimicrobial activity in response to light irradiation. PsPC **9** exhibited the largest increase in photoresponsive activity and the most potent aPDT effect (MIC and MBC of 1.6 μM). The Gly linker in PsPC **9** was changed to PEG4 to examine whether activity enhancement could be observed, as seen in PsPC **1** and **6**. Compared to PsPC **9**, PEG4-linked PsPC **11** exhibited stronger antimicrobial activity in dark conditions, but no photoresponsive activity increase was observed.

The singlet oxygen generated upon light irradiation damages vital membrane components of bacteria only if sufficient amounts are present near the bacterial outer mem-

Table 2 Photophysical properties of 9 and TMPyP (16) in deuterium oxide

Compound	ε [a] (M^{-1} cm^{-1})	Φ_F [b]	Φ_Δ [c]	τ_F [d] (ns)	τ_Δ [e] (ns)
9	1.8×10^5	0.07	0.85	11.9	67.9
TMPyP (**16**)	2.6×10^5	0.06	0.90	6.1	69.9

[a] ε: extinction coefficients at 426 nm (**9**) and 421 nm (**16**). [b] Φ_F: relative fluorescence quantum yield (TPP in DMF was used as a standard; Φ = 0.11).[63] [c] Φ_Δ: relative singlet oxygen quantum yield (TMPyP in D_2O was used as a standard; Φ = 0.90).[53] [d] τ_F: fluorescence emission lifetime at 715 nm. [e] τ_Δ: singlet oxygen phosphorescence emission lifetimes at 1275 nm.

brane.[22] Due to the short half-life of singlet oxygen in aqueous media (Table 2),[59] the decrease in cytotoxicity is generally observed as the distance between the singlet oxygen source and the targeting site of bacteria. It can be inferred that **9** and **10** were localized on the bacterial membrane, and subsequent singlet oxygen generation induced damage to the bacteria. Since the helical antimicrobial peptoid can penetrate the membrane and induce intracellular biomass flocculation,[60] it is also reasonable to assume that **9** and **10** can damage the intracellular components. Further experiments were conducted to clarify the origin of their photoresponsive antimicrobial activity.

The concentration-dependent photoresponsive antimicrobial activity of PsPC (**1**, **9**, and **10**) was more rapidly increased than those of TMPyP (**16**) and peptoids (**12**, **14**, and **15**; Fig. 2a). The growth of bacteria was not disturbed under the given conditions unless the compounds were treated, showing 5 log cell counts. The antimicrobial activity of TMPyP (**16**) barely changed depending on its concentration. Considering that TMPyP (**16**) itself does not have enough affinity for the bacterial membrane without peptoids and that the singlet oxygen lifetime is short (*i.e.*, ~3 μs),[59] it is reasonably speculated that the singlet oxygen generated by TMPyP (**16**) was quenched before reaching the membrane. Peptoids **12**, **14**, and **15** showed a decrease in their activity similar to that reported,[52] indicating that the activity was not significantly affected by light irradiation. However, PsPCs **1**, **9**, and **10** showed complete killing at a much lower concentration than both TMPyP (**16**) and the corresponding peptoids (**12**, **14**, and **15**), which exist independently. This result implies that the conjugation provided a synergistic effect, which induced targeting to the bacterial membrane followed by damage to the structure by generated singlet oxygen.

The relationship between PsPC and the degree of membrane association was confirmed by washing the cells before light irradiation. According to Gobbo and coworkers, the CFU counts recovered when the photosensitizer–AMP conjugates weakly bound to the bacterial membrane were removed during the washing step.[33] The same experiment was performed with PsPCs, which showed a recovery of CFU counts after the washing step (Fig. 2b). PsPC **1** showed a recovery of CFU counts of less than one log scale, whereas PsPCs **9** and **10** resulted in 3 and 1.5 log scale recoveries of CFU counts, respectively. These results suggest that PsPCs **9** and **10** were weakly associated with the bacterial membrane, which greatly affects their photoinduced antimicrobial activity.

Spectroscopic studies of PsPCs

The photophysical and conformational properties of the prepared compounds were investigated by UV-vis absorption, fluorescence emission, phosphorescence and CD spectroscopy

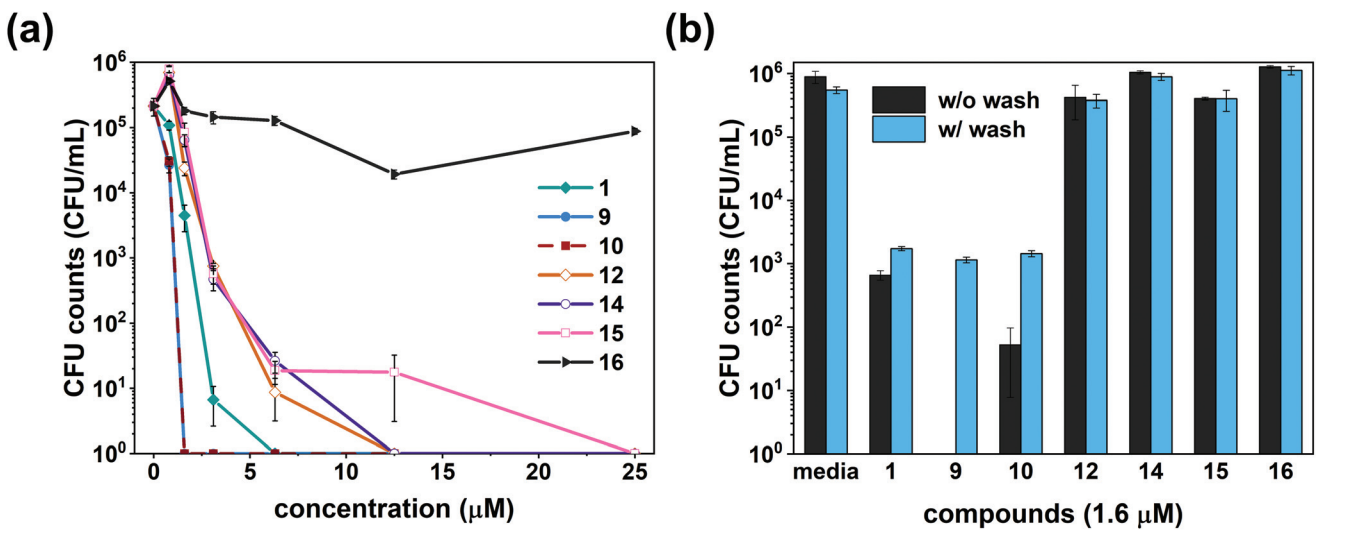

Fig. 2 (a) Concentration-dependent growth inhibition of *E. coli* (ATCC 25922). After blue light irradiation for 15 min (390–460 nm, 420 nm max, 15.1 J cm^{-2}), the cells were cultured overnight at 37 °C. **1**, **9** and **10** are PsPCs. **12**, **14** and **15** are peptoids alone. **16** is TMPyP. (b) Effect of the washing step on antimicrobial photoinactivation against *E. coli* (ATCC 25922). After preincubation of the cells with compounds (1.6 μM) in the dark for 2 h, the cells were washed with MHB2 media (pH 7.4) three times and irradiated following the above conditions in (a). "w/o wash" indicates no buffer washing step between preincubation and light irradiation.

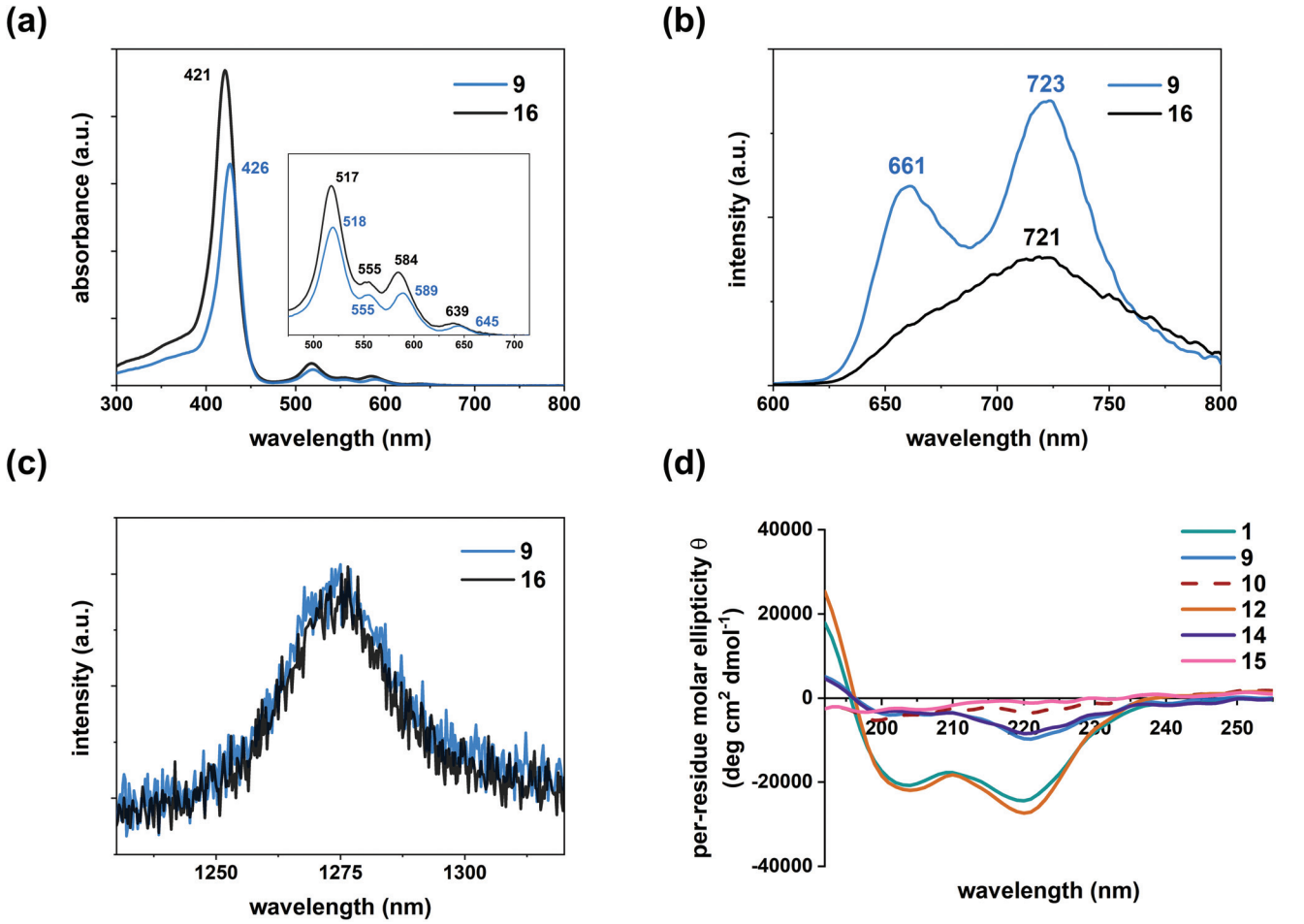

Fig. 3 (a) UV-vis absorption spectra obtained for PsPC **9** and TMPyP **16** (D_2O, 10 μM, 20 °C). The inset represents the Q-band absorption region (475–715 nm). (b) Fluorescence emission spectra of PsPC **9** (0.75 μM) and TMPyP **16** (0.50 μM; D_2O, 20 °C, λ_{ex} = 405 nm). (c) Phosphorescence emission spectra of singlet oxygen generated by PsPC **9** (0.75 μM) and TMPyP **16** (0.50 μM; D_2O, 20 °C, λ_{ex} = 425 nm). (d) CD spectra obtained for PsPCs (**1**, **9**, and **10**) and peptoids (**12**, **14**, and **15**) in 10 mM Tris-HCl buffer (pH 7.0; 50 μM, 20 °C).

(Fig. 3). The absorption properties of PsPC **9** were similar to those of TMPyP (**16**), aside from a decrease in the extinction coefficient (ε) and a slight redshift of peaks (Fig. 3a and Table 2). The UV-vis spectrum of **9** showed a sharp Soret band (λ_{max} = 426 nm) and four distinctive Q-bands (480–700 nm), which is a distinctive feature of a porphyrin.[61] No *J*- or *H*-type aggregation was observed in the Soret region under the conditions used.

Fluorescence emission spectroscopy was conducted to measure the characteristics upon excitation (Fig. 3b and Table 2). The emission spectrum of **9** was clearly resolved into two hills with peaks at 661 nm and 723 nm, while that of TMPyP (**16**) showed a single peak at 721 nm with a shoulder near 665 nm (Fig. 3b), a peak shape reminiscent of previously reported supramolecular assemblies with TMPyP.[61,62] The fluorescence lifetime (τ_F) of **9** was approximately twice as high as that of TMPyP (**16**), and the fluorescence quantum yield (Φ_F) of **9** was slightly higher (Table 2). Conjugation of TMPyP to the peptoid may hamper the assembly of the dyes in aqueous media and modulate the intramolecular charge transfer pathways in TMPyP, thereby forming a new photosensitizer complex with different fluorescence characteristics.

The phosphorescence emission spectra showed that PsPC **9** generated singlet oxygen (Fig. 3c). PsPC **9** and TMPyP (**16**) were dissolved in deuterium oxide for direct observation of singlet oxygen through their characteristic emission (~1275 nm) in an aqueous environment. The excitation wavelength was 425 nm, at which point porphyrin was dominantly excited. Both **9** and TMPyP (**16**) exhibited characteristic emission at approximately 1275 nm, indicating radiative relaxation of singlet oxygen (*i.e.*, $a^1\Delta_g \rightarrow X^3\Sigma_g^-$).[59] The singlet oxygen lifetime (τ_Δ) of TMPyP (**16**) matched that of a previous report,[53] and the singlet oxygen lifetime of **9** was similar to that of TMPyP (Table 2). The quantum yield of singlet oxygen generation (Φ_Δ) was slightly reduced in **9** compared to that in TMPyP (Table 2),[53] which might be the result of quenching due to the nearby peptoid. Taken together, these results show that **9** is a complex with different fluorescence characteristics from those of TMPyP (**16**) but generates singlet oxygen as much as TMPyP (**16**) does upon excitation.

The conformation of PsPCs was analyzed by CD spectroscopy (Fig. 3d). Peptoids composed of α-chiral aromatic side chains (*e.g.*, *N*spe) show polyproline type I (PPI)-like helical structures.[56,57] The characteristic peaks are observed by their carbonyl $\pi \rightarrow \pi^*$ (~192 nm and ~202 nm) and $n \rightarrow \pi^*$ (~220 nm) transitions in the CD spectra.[56,57] Peptoid **12**, composed of 8 *N*spes, indicates a fully helical conformation (Fig. 3d). As previously reported, peptoids **14** and **15** exhibit weakly helical and nonhelical conformations.[52,58] The helicity of the conjugates was not significantly affected by TMPyP conjugation. All PsPCs showed a degree of helicity similar to that of the corresponding peptoids (*i.e.*, fully helical (**1**), weakly helical (**9**), and nonhelical (**10**)), without significant peak shifts (Fig. 3d). It was confirmed that the conjugation of TMPyP at the *N*-terminus of the peptoids did not induce a dramatic change in the conformational characteristics of the resulting complexes. The features were further investigated in the presence of lipid vesicles representing negatively charged bilayer models of bacterial membranes by mixing 1-palmitoyl-2-oleoyl-*sn-glycero*-3-phosphoethanolamine (POPE) and 1-palmitoyl-2-oleoyl-*sn-glycero*-3-phospho-(1′-*rac*-glycerol) (POPG).[52,64,65] PsPC **9** did not exhibit the characteristic CD signature, while the other conjugates exhibited the same CD signature (Fig. S4†). According to our previous studies, a higher-order self-assembly was predicted for peptoid C (**14**), whereas a monomeric form was observed for peptoid A (**12**), both of which were obtained in an aqueous environment.[52] The similar CD signatures of the PsPCs and peptoids imply that the conformational properties were maintained. Thus, it is speculated that the local concentration of **9** was increased due to aggregate formation, and a subsequent increase in the singlet oxygen concentration induced photoresponsive damage to the bacteria.

Photoinduced membrane damage by PsPCs

Flow cytometry (FCM) experiments were conducted to evaluate the interaction between bacterial membranes and **9**. Bacterial samples were prepared *via* preincubation of the cells for 2 h with **9** in the dark, light irradiation for 15 min, washing with MHB2 media (pH 7.4), and then treatment under two different conditions of FCM analyses. Under the first condition, bacterial cells were stained with only SYBR Green I (SGI), which emits strong green fluorescence when bound to DNA, to count the total number of cells (= total cell count, TCC). Under the second condition, cells were stained with a combination of SGI and propidium iodide (PI). Cells can be stained with PI only when their membrane is damaged because PI is a cell-impermeable nucleic acid-binding dye.[66] The number of intact cells was counted for the latter condition (= intact cell count, ICC). The difference relative to the concentration of **9** and the difference between washed and unwashed cells before the measurements were compared.

The TCC did not significantly differ as the concentration of **9** increased or with washing of the cells before irradiation (Fig. S5 and S6†). In all cells stained with only SGI, a TCC of $\sim 3 \times 10^5$ cells per mL was determined within the region of the polygon (Fig. S5†). It could be inferred that the integrity of cells was not severely damaged (*e.g.*, cell lysis) under the measurement conditions. Experiments with the same concentration (*i.e.*, 1.6 μM) of peptoid C (**14**) or TMPyP (**16**) produced similar results (Fig. S7†).

Bacterial membrane damage caused by **9** under light irradiation was observed through ICC using SGI/PI conditions (Fig. 4). Bacterial cells were observed inside the polygon when the bacterial membrane was intact, as appeared when measuring TCCs (Fig. 4 and S5†). However, the cells were observed outside the polygon (*i.e.*, a decrease in green fluorescence and an increase in red fluorescence) when the bacterial membrane was impaired and stained by PI. The ICC was maintained when the cells were treated with **9** and incubated in the dark but dramatically decreased when the cells were irradiated (Fig. 4 and S7†). These results imply that the membrane was damaged by oxidative stress caused by singlet oxygen generated during irradiation. Membrane-damaged cells were not observed with either peptoid C (**14**) or TMPyP (**16**) treatment (Fig. S7†), suggesting that the conjugation provided a strong synergistic effect. The number of ICCs decreased with an increasing concentration of **9** regardless of the washing step (Fig. 4). An increase in the ICC was observed at the same concentration when the cells were washed (Fig. S6†), indicating that a weak association existed between the bacterial membrane and **9**.

Photoinduced DNA damage by PsPC

Gel electrophoresis was performed to investigate the effect of PsPC on nucleic acids (Fig. 5). The experiment focused on the fate of plasmid DNA (*e.g.*, pUC19) that could be transferred to other bacteria, causing one of the major forms of antibiotic resistance.[67] The marker loaded on the gel confirmed that intact pUC19 has a band located below 2 kb and is known to have a supercoiled form. A larger band showing its original length (*i.e.*, 2686 bp) appeared near 3 kb when the DNA was linearized by a restriction enzyme, *EcoRI*. Distinct band locations result from conformational differences, which induce different migration speeds during electrophoresis.

Plasmid DNA was affected by photoresponsive damage generated by photosensitizers. A supercoiled form of pUC19 was sustained when the compounds were treated in the dark (Fig. 5a). However, the results changed dramatically after irradiation (Fig. 5b). pUC19 treated with **9** resulted in band disappearance, which implies extensive fragmentation of DNA. The DNA either maintained its conformation or linearized after *EcoRI* treatment when treated with peptoid C (**14**) or TMPyP (**16**), respectively.[68]

The results of electrophoresis suggest that **9** is a potential multitarget agent. It is well documented that positively charged porphyrin (*e.g.*, TMPyP) intercalates into negatively charged DNA, which induces DNA lesions by photoresponsive damage.[69] However, long periods of irradiation were required for this mechanism.[70] PsPC **9** resulted in DNA fragmentation with concomitant membrane damage under the same conditions (Fig. 4 and **5**). It could be reasoned that the conjugation of cationic porphyrin with a cationic amphipathic

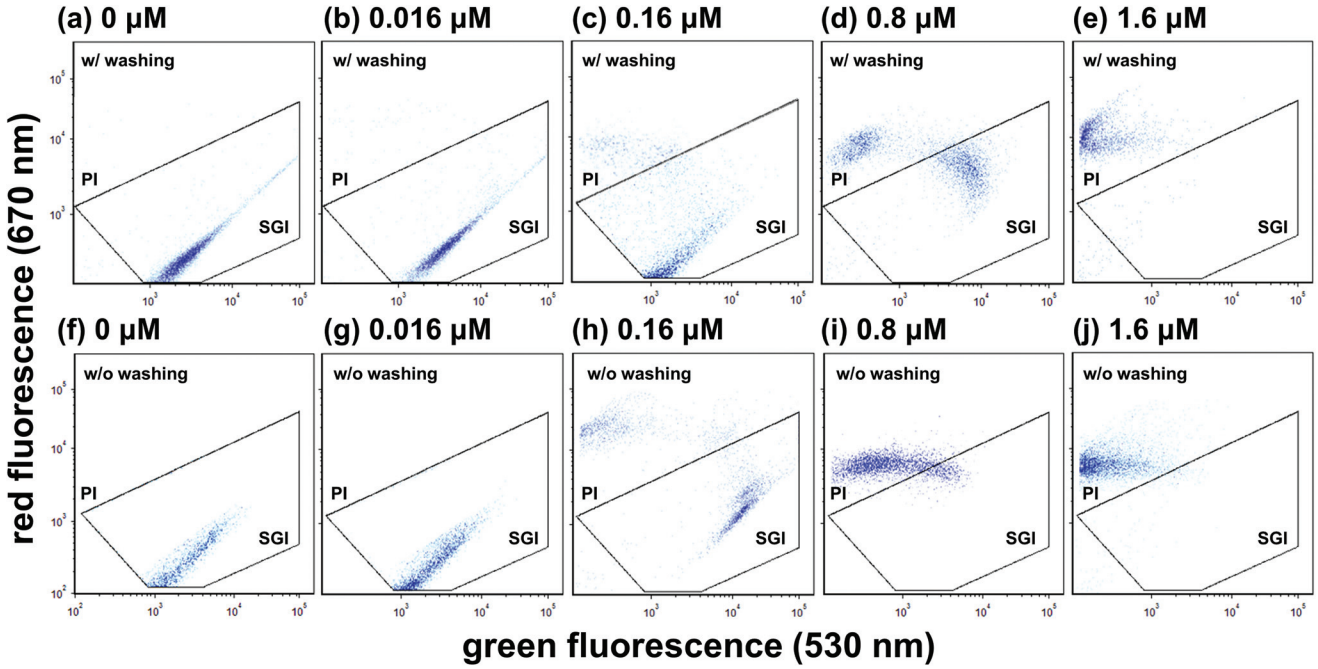

Fig. 4 Flow cytometric density plots (530 nm *vs.* 670 nm) for the ICC changes during aPDT against *E. coli* (ATCC 25922) as a function of the molecular concentration of **9** from zero to 1.6 μM. The samples were prepared with (a–e) or without (f–j) an additional washing step and stained with SGI (10 μL mL^{-1})/PI (0.6 mM) to assess membrane damage. The polygons illustrate gates depicting the region where membrane-intact cells appear.

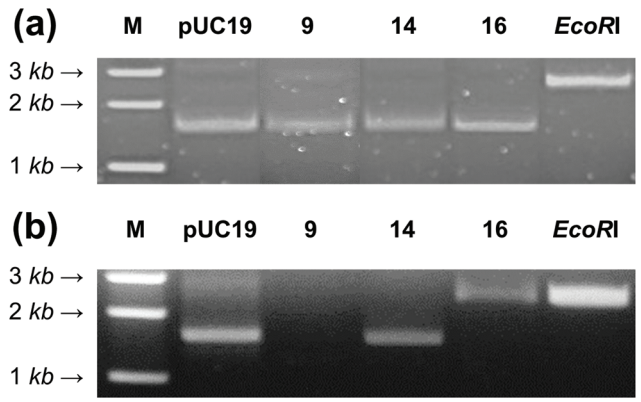

Fig. 5 Agarose gel electrophoresis of extracellular pUC19 plasmids treated with **9** (1.6 μM), peptoid C (**14**; 1.6 μM), and TMPyP (**16**; 1.6 μM) incubated (a) in the dark or (b) under irradiation with blue light for 15 min (390–460 nm, 420 nm max, 15.1 J cm^{-2}). The first column shows the standard DNA ladder. The last column shows the linearized pUC19 after restriction digestion with *EcoR*I.

peptoid (*e.g.*, peptoid C) enhanced the interaction between the conjugate and biomolecules (*e.g.*, membrane and nucleic acids) and the subsequent photoresponsive damage at multiple sites on bacteria with lower conjugate concentrations.

Conclusion

In summary, we synthesized photosensitizer–peptoid conjugates (PsPCs) as aPDT agents and investigated their activity against Gram-negative *E. coli*. A weakly helical peptoid exhibited optimal photoresponsive antimicrobial activity when conjugated with a cationic photosensitizer (*i.e.*, TMPyP), while a fully helical peptoid was less effective when used as a conjugate. PsPC **9** could damage multiple sites on *E. coli*. Bacterial membrane damage was observed when the cells were treated with **9** followed by light irradiation, which demonstrated that the oxidative damage was due to the generated singlet oxygen. The weak association between **9** and the bacterial membrane can explain the photoresponsive inactivation of bacteria. The weakly helical peptoid can be considered "sticky tape" with cationic amphipathic and conformationally flexible properties, which result in an optimal association of PsPC with bacterial membranes. In addition, the decrease in membrane accessibility of peptoids after *N*-terminal porphyrin conjugation can be compensated for by using flexible peptoids rather than using fully structured peptoids. Similar to membrane damage, plasmid DNA damage occurred after treatment with **9** under light irradiation. The fragmented DNA demonstrated that **9** led to oxidative damage to intracellular targets, which had been difficult to achieve with a peptoid or photosensitizer alone. The combined effect of the physicochemical and conformational properties of **9** was crucial for this multitargeting bacterial killing approach.

Although promising antimicrobial agents, PsPCs pose a limitation to overcome. The effective association with the bacterial membrane and subsequent generation of singlet oxygen upon visible light irradiation could provide advantages when utilized for biofilm prevention and irradication,[26] inhibition of fungal spore germination,[71] and wastewater sterilization.[72] The

utility of PsPCs for the above applications certainly calls for further studies. For PsPC to be used in the clinic, we found the current irradiation conditions (*i.e.*, 420 nm, 15.1 J cm^{-2}), the long interval between sample treatment and irradiation (*i.e.*, 2 h preincubation), and cytotoxicity are suboptimal (Table S2†).[22] Thus, our ongoing studies are focused on examining whether selectivity acceptable for clinical use can be attained by expanding the PsPC library and changing the sample treatment conditions, eventually reducing the toxicity. Otherwise, the potential usage of PsPCs will be limited to environmental or device sterilization.

The multitarget bacterial inactivation of PsPC was optimal with conjugation to weakly helical antimicrobial peptoids and cationic photosensitizers. The molecular design and biological activity of PsPCs reported herein are expected to provide insight into the development of next-generation peptoid-based aPDT conjugates.

Experimental section

General information

Reactions were performed in oven-dried (110 °C) glassware under a nitrogen atmosphere unless otherwise noted. Chemicals and solvents were purchased from Sigma-Aldrich (St Louis, MO, USA), Acros Organics (Geel, Belgium), Alfa Aesar (Haverhill, MA, USA), TCI (Tokyo, Japan), or Daejung (Siheung, South Korea) and were used without further purification. Fmoc-Rink Amide MBHA resin (100–200 mesh, 0.52 mmol g^{-1}) was acquired from Merck Millipore (Burlington, MA, USA). Fmoc-*N*-amido-dPEG®$_4$-acid was purchased from Quanta BioDesign (Plain City, OH, USA). Photochlor, verteporfin, and chlorin e6 were acquired from MedKoo Biosciences (Chapel Hill, NC, USA). 1-Palmitoyl-2-oleoyl-*sn-glycero*-3-phosphoethanolamine (POPE) and 1-palmitoyl-2-oleoyl-*sn-glycero*-3-phospho-(1′-*rac*-glycerol) (POPG) were purchased from Avanti Polar Lipids (Alabaster, AL, USA). Flash column chromatography was conducted on silica gel 60 (230–400 mesh, Merck Millipore). The bands were monitored by thin-layer chromatography (TLC) on aluminum-backed TLC sheets (silica gel 60 F254, Merck Millipore). ^{1}H NMR spectra were recorded on a Jeol ECS400 spectrometer (400 MHz). The spectra were referenced to trimethyl silane (0.00 ppm) or residual chloroform (7.26 ppm). Chemical shifts are reported in ppm, and multiplicities are indicated by s (singlet), d (doublet), t (triplet), q (quartet), and m (multiplet). The coupling constants, *J*, are reported in Hertz. Synthetic procedures for photosensitizers, peptoids, and PsPCs were described in the ESI.†

Spectroscopic measurement and analysis

UV-vis spectra were recorded on an Ultrospec 2100 Pro UV-vis spectrophotometer (GE Healthcare, Buckinghamshire, UK) over a range of 300–800 nm in a quartz cell with a 1 cm path length at 20 °C. Baseline correction for each spectrum was carried out with a solvent blank.

Fluorescence emission from PsPCs was measured by a FLS980 fluorescence spectrometer (Edinburgh Instruments, Livingston, UK) with UV-vis PMT (R928P, Hamamatsu, Japan). The steady-state fluorescence spectra were recorded with 405 nm excitation, a 2 nm spectral bandwidth for both excitation and emission, and a 0.1 s dwell time. Ten replicate spectra were obtained and averaged. Time-resolved fluorescence profiles of PsPCs were measured by using the time-correlated single-photon counting (TCSPC) module in FLS980 at an emission wavelength of 715 nm with a 405 nm picosecond pulsed excitation (LDH405, PicoQuant, Germany).

Phosphorescence emission from singlet oxygen was measured by a FLS980 system with a liquid N_2-cooled NIR PMT (R5509-72, Hamamatsu, Japan). Steady-state phosphorescence spectra were recorded with 425 nm excitation, a 0.2 s dwell time, and 4 nm and 15 nm spectral bandwidths for excitation and emission, respectively. Fifty replicate emission spectra were recorded and averaged. Time-resolved phosphorescence emission profiles of singlet oxygen were measured by a multichannel scaling (MCS) module in the FLS980 at an emission wavelength of 1275 nm, synchronized with 425 nm nanosecond excitation pulses from an optical parametric oscillator (MagicPRISM VIR, Opotek, USA) pumped by a Nd:YAG laser (Q-smart 450, Quantel, USA). The typical pulse width was 7 ns, and the repetition rate was 10 Hz. All the emission decay curves were fitted with a single exponential function using MATLAB software.

CD spectra were recorded on a Jasco model 810 spectropolarimeter (Jasco, Easton, MD, USA) in a quartz cell with a 0.2 mm path length. The response time was set to 1 s with a 1.0 nm data pitch and 1.0 nm bandwidth for all spectra. The spectra were acquired in the 190–260 nm range with a 100 nm min^{-1} scanning speed at 20 °C, measured 40 times and averaged. The samples were prepared in either 10 mM Tris-HCl buffer (pH 7.0) or 5 mM lipid vesicles (POPE : POPG = 7 : 3) in 10 mM Tris-HCl buffer (pH 7.0).[57,70] The results were expressed in terms of the per-residue molar ellipticity, $[\theta]$ (deg cm^2 $dmol^{-1}$). ($[\theta] = \theta/(n \times c \times l)$, where θ is the ellipticity of the polarization, n is the number of amide groups present, c is the molar concentration, and l is the optical path length).

Photoinactivation of bacteria

The antimicrobial activity of the compounds was evaluated against both *E. coli* (ATCC 25922) and *S. aureus* (ATCC 25923) and reported as the MIC, which is the lowest concentration of the antimicrobial agent that inhibits the growth of a microorganism after overnight incubation at 37 °C. The minimum bactericidal concentration (MBC), the lowest concentration of the compound that is required to kill bacteria, is also reported. The MIC values of each compound were determined using a broth dilution assay. For each assay, primary cultures of either *E. coli* or *S. aureus* were grown overnight in Mueller Hinton Broth 2 (MHB2, cation-adjusted) medium at 37 °C. A secondary culture was started the next day and grown for 3 to 4 h. The bacteria used in the experiments were collected from cultures in the stationary phase of growth. This culture was then

diluted in MHB2 medium corresponding to approximately (2–5) × 10^5 CFU mL^{-1} bacteria. Using polypropylene 96-well plates (Corning, Corning, NY, USA), 100 μL of (2–5) × 10^5 CFU mL^{-1} bacteria was added in triplicate for each compound. Each compound was assayed at six different concentrations in 2-fold serial dilutions. The plates were wrapped with aluminum foil to block ambient light and placed at 37 °C for 2 h. After incubation in the dark, the suspensions were directly exposed to light (no washing) or centrifuged to wash the unbound compounds left in the suspension. For the washing experiment, the mixture was centrifuged (10 000*g*) for 3 min, and the supernatant was removed. The cells were resuspended in 1 mL of MHB2 medium, and the steps were repeated three times. For light irradiation, aliquots of bacterial samples were transferred into 96-well plates (100 μL per well). Irradiation was performed with blue light (390–460 nm, 420 nm max, 16.8 mW cm^{-2}) emitted by a homemade LED array. The fluence rate was measured with a light meter (FieldMax-II, Coherent, Santa Clara, CA, USA) with an optical sensor (OP-2 UV, Coherent). After irradiation for 15 min, MIC data were recorded by measuring the optical density (OD) at 600 nm on a microplate reader (BioTek Instrument, Winooski, VT, USA). All bacterial solutions remaining on the plates after the MIC assay were spread on a separate agar plate to determine the MBCs. The plates were incubated at 37 °C overnight to confirm bacterial growth. The MBC was determined as the minimum concentration required to prevent bacterial growth on the agar plates. For the colony count assay, bacterial suspensions treated with each compound were serially diluted 10-fold in MHB2 media, and aliquots of the appropriate dilutions (100 μL) were spread in triplicate onto MHB2 agar. The agar plates were further incubated for 24 h at 37 °C to determine CFUs. Pictures of the plates were uploaded to OpenCFU software to count the number of colonies grown on the plates.

Flow cytometry analysis

Flow cytometry (FCM) analysis was performed as described previously.[66,73,74] Briefly, SYBR Green I (SGI, Invitrogen, Carlsbad, CA, USA) was prepared by diluting SGI 100-fold with DMSO. A mixture of SGI and PI (Invitrogen) was prepared by mixing SGI and 30 mM PI at a final PI concentration of 0.6 mM. The working solutions (SGI and SGI/PI) were kept at −20 °C until use. The sample (1 mL) was stained with SGI or SGI/PI at 10 μL mL^{-1} and incubated in the dark for 12 min at 36 °C. Before FCM analysis, samples were diluted with autoclaved water filtered through a 0.2 μm syringe filter (Whatman, Sigma-Aldrich) to 1% or 10% v/v of the initial concentration. FCM analyses were performed using a CyFlow® Cube 6 flow cytometer (Sysmex Korea, Seoul, South Korea) equipped with a 488 nm blue laser. Fluorescence was detected at 530 nm (green) and 670 nm (red). Data were arranged in density plots of 530 nm *versus* 670 nm. Individual dots in the plots reflected the signals for each particle that was a bacterial cell. Bacterial cells were separated from the instrument or sample background noise by electronic gates, which were constructed manually using the supplied FCM software. The cell quantification limits of the FCM methods in this study were ~1000 cells per mL, and the standard deviation of the measurement was below 5%.[74]

Gel electrophoresis

pUC19 plasmids (1 μg mL^{-1}) treated with the compounds under different irradiation conditions were analyzed by gel electrophoresis to assess the structural changes in plasmid DNA (*i.e.*, supercoiled, linearized, or open-circular formed). Linearized pUC19 was prepared for use as a reference by incubating the plasmid with the type II restriction enzyme *EcoRI* (NEB, USA) at 37 °C for 1 h, followed by enzyme inactivation at 65 °C for 20 min. After irradiation, the samples and a 1 kb DNA ladder (Enzynomics, Daejeon, South Korea) were loaded on 0.8% agarose gels at 4 V cm^{-2} for 35 min. The bands were visualized by ethidium bromide staining. Gel images were captured on a UV transilluminator (Universal mutation detection system, UVP, Upland, CA, USA).

Author contributions

W. Yang, Y. Yoon, Y. Lee, and H. Oh contributed equally to this work. Y. Lee and J. Seo conceived and directed the project. W. Yang and Y. Lee synthesized and characterized the compounds. W. Yang and J. Choi conducted the biological assays. W. Yang and H. Oh performed spectroscopic analyses. Y. Yoon, J. Choi and S. Shin conducted the flow cytometry experiments and DNA gel electrophoresis. S. Lee provided the homemade LED array. J. Seo, Y. Lee, H. Lee, W. Yang, and Y. Yoon wrote the manuscript with contribution from all authors.

Conflicts of interest

There are no conflicts to declare.

Acknowledgements

This work was financially supported by the National Research Foundation of Korea (NRF-2018R1A2B6007535, 2018M3D1A1052659, 2021R1A2C2014421 to J. S.), Korea Basic Science Institute (D110720 to S. L.) and by the GIST Research Institute (GRI) GIST-CNUH Research Collaboration grant funded by GIST in 2021.

References

1 D. A. Gray and M. Wenzel, *ACS Infect. Dis.*, 2020, **6**, 1346–1365.
2 D. J. Scheffers and M. G. Pinho, *Microbiol. Mol. Biol. Rev.*, 2005, **69**, 585–607.
3 M. Teuber and J. Bader, *Arch. Microbiol.*, 1976, **109**, 51–58.

4 K. L. Tyrrell, D. M. Citron, Y. A. Warren and E. J. Goldstein, *Antimicrob. Agents Chemother.*, 2012, **56**, 2194–2197.
5 A. L. Parkes and I. A. Yule, *Expert Opin. Drug Discovery*, 2016, **11**, 665–680.
6 H. H. Locher, P. Seiler, X. H. Chen, S. Schroeder, P. Pfaff, M. Enderlin, A. Klenk, E. Fournier, C. Hubschwerlen, D. Ritz, C. P. Kelly and W. Keck, *Antimicrob. Agents Chemother.*, 2014, **58**, 892–900.
7 M. U. Rashid, A. Dalhoff, A. Weintraub and C. E. Nord, *Anaerobe*, 2014, **28**, 216–219.
8 Z. K. Ma and A. S. Lynch, *J. Med. Chem.*, 2016, **59**, 6645–6657.
9 X. Y. Kang, F. Y. Dong, C. Shi, S. C. Liu, J. Sun, J. X. Chen, H. Q. Li, H. M. Xu, X. Z. Lao and H. Zheng, *Sci. Data*, 2019, **6**, 148.
10 U. H. N. Durr, U. S. Sudheendra and A. Ramamoorthy, *Biochim. Biophys. Acta, Biomembr.*, 2006, **1758**, 1408–1425.
11 K. Matsuzaki, K. Sugishita, M. Harada, N. Fujii and K. Miyajima, *Biochim. Biophys. Acta, Biomembr.*, 1997, **1327**, 119–130.
12 M. Sinha, S. Kaushik, P. Kaur, S. Sharma and T. P. Singh, *Int. J. Pept.*, 2013, **2013**, 390230.
13 B. Bechinger and S. U. Gorr, *J. Dent. Res.*, 2017, **96**, 254–260.
14 C. F. Le, C. M. Fang and S. D. Sekaran, *Antimicrob. Agents Chemother.*, 2017, **61**, e02340–e02316.
15 C. H. Chen and T. K. Lu, *Antibiotics*, 2020, **9**, 24.
16 J. B. Bhonsle, T. Clark, L. Bartolotti and R. P. Hicks, *Curr. Top. Med. Chem.*, 2013, **13**, 3205–3224.
17 Z. Liu, A. Brady, A. Young, B. Rasimick, K. Chen, C. Zhou and N. R. Kallenbach, *Antimicrob. Agents Chemother.*, 2007, **51**, 597–603.
18 M. Dathe, H. Nikolenko, J. Klose and M. Bienert, *Biochemistry*, 2004, **43**, 9140–9150.
19 A. Jodlbauer and H. von Tappeiner, *Muench. Med. Wochenschr.*, 1904, **51**, 1096–1097.
20 F. Cieplik, D. M. Deng, W. Crielaard, W. Buchalla, E. Hellwig, A. Al-Ahmad and T. Maisch, *Crit. Rev. Microbiol.*, 2018, **44**, 571–589.
21 C. S. Foote, *Photochem. Photobiol.*, 1991, **54**, 659.
22 F. Vatansever, W. C. M. A. de Melo, P. Avci, D. Vecchio, M. Sadasivam, A. Gupta, R. Chandran, M. Karimi, N. A. Parizotto, R. Yin, G. P. Tegos and M. R. Hamblin, *FEMS Microbiol. Rev.*, 2013, **37**, 955–989.
23 E. Alves, M. A. Faustino, J. P. Tome, M. G. Neves, A. C. Tome, J. A. Cavaleiro, A. Cunha, N. C. Gomes and A. Almeida, *Bioorg. Med. Chem.*, 2013, **21**, 4311–4318.
24 E. Alves, A. C. Esteves, A. Correia, A. Cunha, M. A. F. Faustino, M. G. P. M. S. Neves and A. Almeida, *Photochem. Photobiol. Sci.*, 2015, **14**, 1169–1178.
25 A. Gollmer, A. Felgentrager, W. Baumler, T. Maisch and A. Spath, *Photochem. Photobiol. Sci.*, 2015, **14**, 335–351.
26 T. L. Collins, E. A. Markus, D. J. Hassett and J. B. Robinson, *Curr. Microbiol.*, 2010, **61**, 411–416.
27 L. N. Dovigo, J. C. Carmello, M. T. Carvalho, E. G. Mima, C. E. Vergani, V. S. Bagnato and A. C. Pavarina, *Biofouling*, 2013, **29**, 1057–1067.
28 A. P. D. Ribeiro, M. C. Andrade, V. S. Bagnato, C. E. Vergani, F. L. Primo, A. C. Tedesco and A. C. Pavarina, *Lasers Med. Sci.*, 2015, **30**, 549–559.
29 T. Maisch, A. Eichner, A. Spath, A. Gollmer, B. Konig, J. Regensburger and W. Baumler, *PLoS One*, 2014, **9**, e111792.
30 C. Ringot, V. Sol, M. Barriere, N. Saad, P. Bressollier, R. Granet, P. Couleaud, C. Frochot and P. Krausz, *Biomacromolecules*, 2011, **12**, 1716–1723.
31 M. A. Castriciano, R. Zagami, M. P. Casaletto, B. Martel, M. Trapani, A. Romeo, V. Villari, M. T. Sciortino, L. Grasso, S. Guglielmino, L. M. Scolaro and A. Mazzaglia, *Biomacromolecules*, 2017, **18**, 1134–1144.
32 J. H. Wang, H. Wu, Y. M. Yang, R. Yan, Y. Zhao, Y. H. Wang, A. H. Chen, S. L. Shao, P. J. Jiang and Y. Q. Li, *Nanoscale*, 2018, **10**, 132–141.
33 R. Dosselli, C. Tampieri, R. Ruiz-Gonzalez, S. De Munari, X. Ragas, D. Sanchez-Garcia, M. Agut, S. Nonell, E. Reddi and M. Gobbo, *J. Med. Chem.*, 2013, **56**, 1052–1063.
34 R. Dosselli, R. Ruiz-Gonzalez, F. Moret, V. Agnolon, C. Compagnin, M. Mognato, V. Sella, M. Agut, S. Nonell, M. Gobbo and E. Reddi, *J. Med. Chem.*, 2014, **57**, 1403–1415.
35 F. Le Guern, V. Sol, C. Ouk, P. Arnoux, C. Frochot and T. S. Ouk, *Bioconjugate Chem.*, 2017, **28**, 2493–2506.
36 F. Le Guern, T. S. Ouk, C. Ouk, R. Vanderesse, Y. Champavier, E. Pinault and V. Sol, *ACS Med. Chem. Lett.*, 2018, **9**, 11–16.
37 F. Liu, A. S. Y. Ni, Y. Lim, H. Mohanram, S. Bhattacharjya and B. G. Xing, *Bioconjugate Chem.*, 2012, **23**, 1639–1647.
38 J. Zhou, G. B. Qi and H. Wang, *J. Mater. Chem. B*, 2016, **4**, 4855–4861.
39 L. Bourre, F. Giuntini, I. M. Eggleston, C. A. Mosse, A. J. MacRobert and M. Wilson, *Photochem. Photobiol. Sci.*, 2010, **9**, 1613–1620.
40 Y. Luo, H. L. Bolt, G. A. Eggimann, D. F. McAuley, R. McMullan, T. Curran, M. Zhou, C. A. B. Jahoda, S. L. Cobb and F. T. Lundy, *ChemBioChem*, 2017, **18**, 111–118.
41 R. N. Zuckermann, J. M. Kerr, S. B. H. Kent and W. H. Moos, *J. Am. Chem. Soc.*, 1992, **114**, 10646–10647.
42 A. S. Culf and R. J. Ouellette, *Molecules*, 2010, **15**, 5282–5335.
43 N. P. Chongsiriwatana, J. A. Patch, A. M. Czyzewski, M. T. Dohm, A. Ivankin, D. Gidalevitz, R. N. Zuckermann and A. E. Barron, *Proc. Natl. Acad. Sci. U. S. A.*, 2008, **105**, 2794–2799.
44 N. Molchanova, P. R. Hansen and H. Franzyk, *Molecules*, 2017, **22**, 1430.
45 K. L. Bicker and S. L. Cobb, *Chem. Commun.*, 2020, **56**, 11158–11168.
46 B. Findlay, P. Szelemej, G. G. Zhanel and F. Schweizer, *PLoS One*, 2012, **7**, e41141.
47 J. Lee, D. Kang, J. Choi, W. Huang, M. Wadman, A. E. Barron and J. Seo, *Bioorg. Med. Chem. Lett.*, 2018, **28**, 170–173.

48 B. Mojsoska, G. Carretero, S. Larsen, R. V. Mateiu and H. Jenssen, *Sci. Rep.*, 2017, **7**, 42332.
49 R. Shyam, N. Charbonnel, A. Job, C. Blavignac, C. Forestier, C. Taillefumier and S. Faure, *ChemMedChem*, 2018, **13**, 1513–1516.
50 R. D. Jahnsen, A. Sandberg-Schaal, K. J. Vissing, H. M. Nielsen, N. Frimodt-Moller and H. Franzyk, *J. Med. Chem.*, 2014, **57**, 2864–2873.
51 M. L. Huang, S. B. Shin, M. A. Benson, V. J. Torres and K. Kirshenbaum, *ChemMedChem*, 2012, **7**, 114–122.
52 H. Y. Nam, J. Choi, S. D. Kumar, J. E. Nielsen, M. Kyeong, S. Wang, D. Kang, Y. Lee, J. Lee, M. H. Yoon, S. Hong, R. Lund, H. Jenssen, S. Y. Shin and J. Seo, *ACS Infect. Dis.*, 2020, **6**, 2732–2744.
53 R. W. Redmond and J. N. Gamlin, *Photochem. Photobiol.*, 1999, **70**, 391–475.
54 Q. Z. Zhang, J. He, W. M. Yu, Y. C. Li, Z. H. Liu, B. N. Zhou and Y. M. Liu, *RSC Med. Chem.*, 2020, **11**, 427–437.
55 M. Ali-Seyed, R. Bhuvaneswari, K. C. Soo and M. Olivo, *Int. J. Oncol.*, 2011, **39**, 821–831.
56 P. Armand, K. Kirshenbaum, A. Falicov, R. L. Dunbrack, K. A. Dill, R. N. Zuckermann and F. E. Cohen, *Folding Des.*, 1997, **2**, 369–375.
57 K. Kirshenbaum, A. E. Barron, R. A. Goldsmith, P. Armand, E. K. Bradley, K. T. V. Truong, K. A. Dill, F. E. Cohen and R. N. Zuckermann, *Proc. Natl. Acad. Sci. U. S. A.*, 1998, **95**, 4303–4308.
58 H. M. Shin, C. M. Kang, M. H. Yoon and J. Seo, *Chem. Commun.*, 2014, **50**, 4465–4468.
59 E. Skovsen, J. W. Snyder, J. D. C. Lambert and P. R. Ogilby, *J. Phys. Chem. B*, 2005, **109**, 8570–8573.
60 N. P. Chongsiriwatana, J. S. Lin, R. Kapoor, M. Wetzler, J. A. C. Rea, M. K. Didwania, C. H. Contag and A. E. Barron, *Sci. Rep.*, 2017, **7**, 16718.
61 E. Reddi, M. Ceccon, G. Valduga, G. Jori, J. C. Bommer, F. Elisei, L. Latterini and U. Mazzucato, *Photochem. Photobiol.*, 2002, **75**, 462–470.
62 R. Khurana, A. S. Kakatkar, S. Chatterjee, N. Barooah, A. Kunwar, A. C. Bhasikuttan and J. Mohanty, *Front. Chem.*, 2019, **7**, 452.
63 P. G. Seybold and M. Gouterman, *J. Mol. Spectrosc.*, 1969, **31**, 1–13.
64 J. A. Patch and A. E. Barron, *J. Am. Chem. Soc.*, 2003, **125**, 12092–12093.
65 K. Murzyn, T. Rog and M. Pasenkiewicz-Gierula, Phosphatidylethanolamine-phosphatidylglycerol bilayer as a model of the inner bacterial membrane, *Biophys. J.*, 2005, **88**, 1091–1103.
66 F. Hammes, M. Berney, Y. Y. Wang, M. Vital, O. Koster and T. Egli, *Water Res.*, 2008, **42**, 269–277.
67 C. M. Thomas and K. M. Nielsen, *Nat. Rev. Microbiol.*, 2005, **3**, 711–721.
68 R. J. Fiel, N. Datta-Gupta, E. H. Mark and J. C. Howard, *Cancer Res.*, 1981, **41**, 3543–3545.
69 B. R. Munson and R. J. Fiel, *Nucleic Acids Res.*, 1992, **20**, 1315–1319.
70 D. A. Caminos, M. B. Spesia, P. Pons and E. N. Durantini, *Photochem. Photobiol. Sci.*, 2008, **7**, 1071–1078.
71 A. Preuss, I. Saltsman, A. Mahammed, M. Pfitzner, I. Goldberg, Z. Gross and B. Roder, *J. Photochem. Photobiol., B*, 2014, **133**, 39–46.
72 M. Bartolomeu, S. Reis, M. Fontes, M. G. P. M. S. Neves, M. A. F. Faustino and A. Almeida, *Water Res.*, 2017, **9**, 630.
73 M. H. Phe, M. Dossot, H. Guilloteau and J. C. Block, *Water Res.*, 2005, **39**, 3618–3628.
74 Y. Yoon, H. J. Chung, D. Y. W. Di, M. C. Dodd, H. G. Hur and Y. Lee, *Water Res.*, 2017, **123**, 783–793.